JTTEE5 21:121–131
DOI: 10.1007/s11666-011-9692-3
1059-9630/$19.00 © ASM International



# Behavior of Calcia-Stabilized Zirconia Coating at High Temperature, Deposited by Air Plasma Spraying System

*M. Billah Bhatty, F. Ahmad Khalid, and A. Nusair Khan*

*(Submitted June 2, 2011; in revised form August 10, 2011)*

**Thermal barrier coatings (TBCs) are employed to protect metallic components from heat, oxidation, and corrosion in hostile environments. In this paper Ni-20Cr bond coat followed by $CaZrO_3$ top coat was deposited on 316 stainless steel substrates by air plasma spray coating technique. Isothermal treatment of coated samples was carried out to investigate the effect of heat exposure on the microstructure and metallurgical phase changes of TBCs system. The fractured surface of as-sprayed and delaminated $CaZrO_3$ coatings was also studied to observe the splats morphology, structural defects, and lamellas internal microstructure. $CaZrO_3$ coating was found to be stable for 100 h at 700 °C but accelerated degradation was observed at 900 °C even at 20 h and lead to delamination after 60 h of exposure time. Chromium rich oxide formation was found to be responsible for the complete delamination of the top coat. Further, the formation of meta-stable monoclinic phase was also observed on the top surface of the top coat.**

**Keywords** calcia-stabilized zirconia, nickel rich bond coat, plasma spraying

## 1. Introduction

Many industrial processes work in highly hostile environments such as high temperature, high pressure, fluctuating stresses (mechanical loads), etc., which are also oxidizing and corrosive in nature. Gas turbine engine used in power generation, aircraft, and marine propulsion are few examples of these processes (Ref 1–3). Metallic parts used in such processes should have the capability to endure harsh environment without failure. Stainless steels and superalloys are the candidate materials for some diesel engines and gas turbines, respectively, and since 1965 a lot of progress has been made in developing alloys for high temperature applications (Ref 4, 5). The superalloys with excellent properties of high-temperature strength, oxidation and hot-corrosion resistance have been used in polycrystalline, directionally solidified and single crystal forms at the maximum limit but cannot survive in extreme conditions due to high working temperature (close to melting point of alloys) and oxidation/corrosion failure (Ref 2, 6). This shows that strengthening of alloys cannot contribute fully to avoid component damage. The possible solution to improve and extend the life of materials is the coating technology. Thermal barrier coatings (TBCs) system protects the metallic components from heat, wear, oxidation, and corrosion (Ref 7–13). The TBCs system makes it possible to improve the component life and performance by either reducing its surface temperature (~170–200 °C) or by increasing gas temperature (~100–300 °C) which results in fuel saving and increases the engine thrust and efficiency up to 5 and 1%, respectively (Ref 3–8, 10–12, 14–20).

TBCs system has complex structure and usually consists of four layers, metallic substrate, bond coat (BC), thermally grown oxide layer (TGO), and top coat (TC) (Ref 18). It has been reported that at high temperature, oxygen and some destructive species are transported through ceramic top coat which can damage metallic parts (Ref 6, 15, 21). Metallic bond coat, 70–150 μm in thickness is used to protect the substrate from high temperature oxidation and corrosion. It improves adhesion of ceramic top coating by providing rough surface for mechanical bonding and further minimizes the coefficient of thermal expansion (CTE) mismatch between substrate and top coat (Ref 4, 22). The typical bond coat materials used in TBC systems are Ni-Cr, Ni-Al, Ni-Cr-Al, Ni-Al(Pt), MCrAlY (M = Ni, Co or Ni + Co) (Ref 6). The NI-20Cr coating has excellent corrosion resistance (i.e., corrosion by sulfur and vanadium at high temperature) and is widely used for the protection of metallic parts in high temperature plants. The mechanical properties of Ni-Cr are good enough and have better adhesion, wear, and erosion resistance (Ref 23). The characteristic properties of top coat are high melting point, excellent thermal stability, good erosion resistance, high CTE, and low thermal conductivity (Ref 6). The candidate

**M. Billah Bhatty** and **F. Ahmad Khalid**, Faculty of Materials Science and Engineering, Ghulam Ishaq Khan Institute of Engineering Sciences and Technology, Topi, Khyber Pakhtunkhaw, Pakistan; and **A. Nusair Khan**, Institute of Industrial and Control Systems, Rawalpindi, Pakistan. Contact e-mail: mustasim63@gmail.com.

materials employed for the top coating of TBC systems are stabilized zirconia. Zirconia can be stabilized by MgO, CaO, $Y_2O_3$, $CeO_2$, etc., and among them $ZrO_2$–$Y_2O_3$ (YSZ) has been recognized as an outstanding material for last few decades but, it is comparatively more expensive (Ref 12, 24, 25). However, in some gas turbines CaO- and MgO-stabilized $ZrO_2$ has been used at high temperature of 1273 K (Ref 25).

Recently, it has been reported that $CaZrO_3$ with perovskite structure has the low thermal conductivity (~2 W/m K) which is even improved as compared to YSZ (Ref 7, 14). Moreover, $CaZrO_3$ is considered as the most stable compound having low cost and showing good corrosion resistance in KOH and mixture of $NaVO_2$ and $Na_2SO_4$ corroding conditions (Ref 26). This shows that $CaZrO_3$ has the great potential to be used as top coat materials for appropriate applications. The use of $CaZrO_3$ plasma coating in diesel engine for the combustion chamber, cylinder head, and valve has been reported to reduce the heat losses to cooling system, enhancement in component life, fuel saving, and improvement in thermal efficiency (Ref 27, 28).

In the previous work on $CaZrO_3$ coatings no systematic research has been conducted to study effect of long elevated temperature exposure on their life and durability. In the present study the TBC system consists of stainless steel substrate on which Ni-Cr bond coat and top coat of $CaZrO_3$ are deposited by APS process. The atmospheric isothermal treatments of TBC system were carried out to ascertain the effects on their microstructures, phases, and delamination behavior.

**Table 1 Chemical composition of substrate material**

| | Weight percentage | |
|---|---|---|
| **Elements** | **Substrate** | **AISI 316(a)** |
| Fe | Bal | Balance |
| Cr | 17.38 | 16-18 |
| Ni | 10.72 | 10-14 |
| Mo | 1.82 | 2-3 |
| Mn | 1.21 | ≤ 2.0 |
| Si | 0.55 | ≤ 1.0 |

(a) Nearest standard

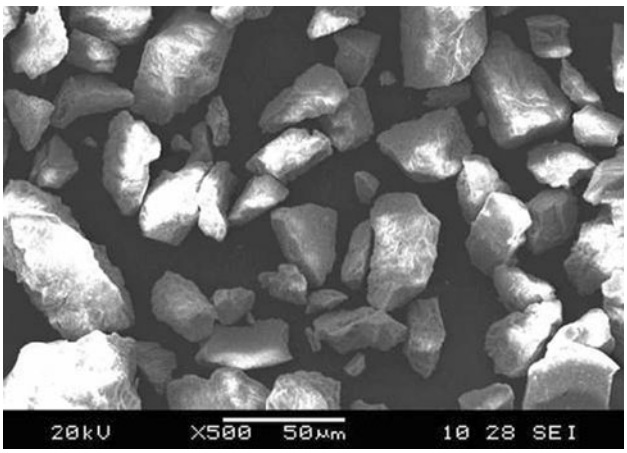


**Fig. 1** $CaZrO_3$ ceramic powder used for top coat

## 2. Experimental

The stainless steel AISI 316 discs of size 25 mm in diameter and 5 mm in thickness were used as substrate material for the coatings. The composition of substrate material is given in Table 1. The substrate was grit blasted with $Al_2O_3$ particles for 4 min and substrate surface roughness of 3.3 to 5.0 µm (Ra) was achieved after grit blasting. During the grit blasting the air pressure was 80 psi and the angle between the substrate surface and nozzle was about at 90°. Air plasma spray (APS) technique was used to deposit both the bond coat and ceramic top coating. For plasma coatings stainless steel cylindrical holder (SCH), 200 mm in diameter and 4 mm in thickness was used to get uniform coatings and good control of substrate temperature. In this SCH there were 32 uniformly distributed holes in which disc-shaped samples were held by screws.

Powder used for bond coat (BC) was Ni-20Cr (wt.%) with average particle size of 40 ± 10 µm. The commercially graded $CaZrO_3$ ceramic powder having composition (wt.%) $ZrO_2$-31CaO was used for top coatings (TC).

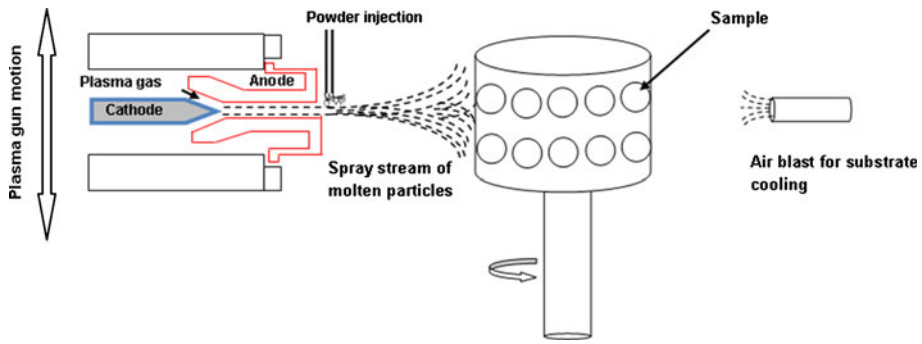


**Fig. 2** Schematic showing the arrangement for APS coating system

**Table 2 Constant spraying parameters for bond coat and top coat**

| Type of coat | Current, A | Voltage, V | Gas flow | | | Feed rate, lbs/h |
|---|---|---|---|---|---|---|
| | | | Primary gas (Ar) (SCFH) | Secondary gas ($H_2$) (SCFH) | Carrier gas (Ar) (SCFH) | |
| Bond coat | 400 | 47 | 180 | 20 | 26 | 14 |
| Top coat | 500 | 48 | 180 | 20 | 40 | 6 |

The $CaZrO_3$ particles were irregular and elongated in shape with average size of 45 ± 15 μm (Fig. 1).

During the plasma coating the samples were rotating at 250 rpm while the plasma torch was moving with uniform speed in to and fro manner along the rotating *x*-axis of SCH (Fig. 2). The plasma gun of 40 kW was used for plasma coatings. The standoff distance for bond coat and ceramic coating was 125 and 100 mm, respectively. Freshly grit blasted samples were air plasma sprayed (APS) and the main parameters of plasma spraying are given in Table 2. The temperature of the substrate during the plasma coatings was maintained at the optimum level by using compressed air at 10 psi pressure. The coating temperature after bond coat and top coat was recorded as 30 and 115 °C, respectively.

For isothermal treatment the coated samples were heat treated in box type furnace at 700, 800, 900, and 1000 °C for 5, 10, 20, 60, and 100 h and then cooled down in the furnace. This long heat treatment was carried out in steps, each having span of 6 h.

The microstructures of the coatings were observed using optical microscope and Jeol Scanning Electron Microscope (SEM). For this purpose the samples were prepared both in cross-sectional direction and top direction. For analyzing the ceramic coatings in SEM, gold was sputtered on the polished surfaces of samples to make them conductive. Chemical composition profiles in heat treated and as-sprayed sample were determined by Energy Dispersive Spectroscopy (EDS). Further the fractured surface and top surface of the coatings was also observed under the SEM. Philips X-ray diffractometer (XRD) using Cu Kα source was used to determine the phases in the coating system in as sprayed and heat treated condition.

## 3. Results and Discussion

### 3.1 Microstructure of Coating System

**3.1.1 As-Sprayed Coating.** The top surface of $CaZrO_3$ coating of as-sprayed sample demonstrated rough surface with few semi-molted particles (SMP), Fig. 3. Further, cracks and porosity like features were also observed in the same surface. These are typically observed in these types of ceramic coatings (Ref 29).

The cross-section of the as-sprayed coating system demonstrates the thickness of top coat and bond coat, Fig. 4a. It revealed that the top coat and bond coat have 180 ± 20 and 70 ± 10 μm thickness, respectively. In general, the top coat has porosity with lamellar structure,

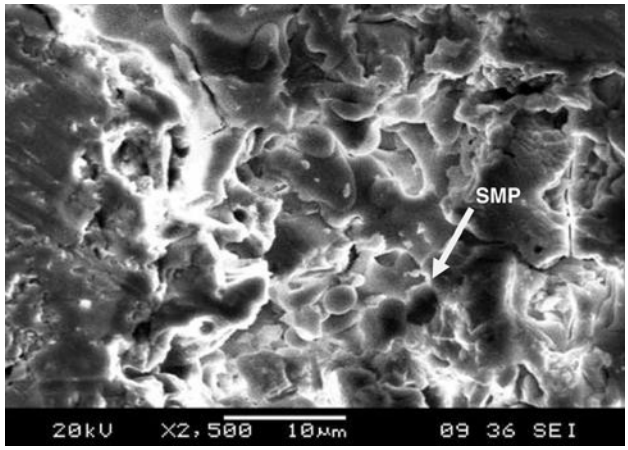


**Fig. 3** As-sprayed coating showing the top view of the top coat

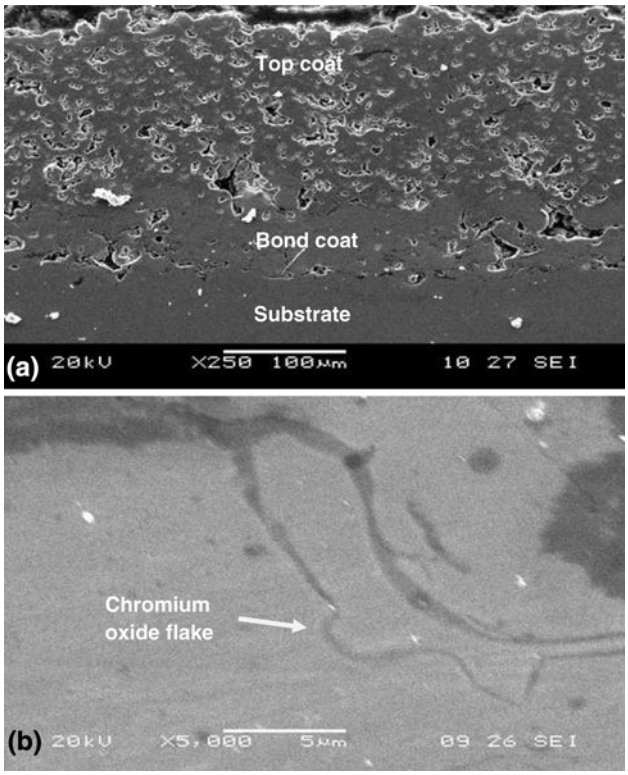


**Fig. 4** (a) Cross-section of the as-sprayed coating showing the thickness and general features of bond coat and top coat. (b) Oxidized chromium flakes in the bond coat

Fig. 4a. It was observed that some grayish flake-like features (~0.2 μm thick) were present in the bond coat, Fig. 4b. These were confirmed by EDS and were found rich in chromium and oxygen contents. The chromium oxide was probably formed during the air plasma spraying. This is also true for other types of bond coats sprayed by this technique (Ref 30, 31).

**3.1.2 Microstructure After Heat Treatment.** The samples exposed at 700 °C for 100 h demonstrated that there was no significant affect on the coating system. Figure 5 shows the cross section of the sample heat treated at 700 °C for 100 h. It was observed that for this heat treatment cycle, the interface of bond coat and top coat remained intact and stable. Moreover no crack was observed in the topcoat. A chromium-rich oxidized layer was identified close to the interface of bond coat and top coat whereas its thickness was about ~0.9 μm (Fig. 5). This layer was not observed in as-sprayed system. The thickness of chromium-rich oxidized layer increased to ~1.5 μm, when the samples were exposed at 800 °C for 100 h, Fig. 6. Further, on closely observing the sample exposed at 800 °C for 100 h it revealed that a crack was initiated as shown in Fig. 7. The cracking seemed to be started from the interface of bond coat and top coat.

Some type of crack was observed after 10 h when the samples were exposed at 900 °C (Fig. 8a) and became evident after 20 h (Fig. 8b). This delamination occurred close to the interface of bond coat and top coat. The delaminated side of the coating was investigated under SEM for analyzing its composition and microstructure. Figure 9 shows the schematic view of the delaminated top coat.

On observing the bond coat side of delaminated top coat, it was observed that the patches of the bond coat were present along with the fractured calcium zirconate top coat. These bond coat patches had isolated zones of chromium oxide, Fig. 10.

This leads to the fact that the formation of chromium oxide at the interface of bond coat and top coat played an important role in the delamination of top coat. It was observed that the Cr-rich oxide layer continuously grew at the interface of the bond coat and top coat with temperatures, Fig. 11.

It was noted that the effect of temperature was not significant at 700 and 800 °C but has a pronounced effect at 900 and 1000 °C. It is worth to mention here that in Fig. 11, the values at 700 and 800 °C are taken after exposure of 100 h, while at 900 °C (Fig. 8b) and 1000 °C (Fig. 12) are after 20 h. This is because the coating of samples exposed at 900 and 1000 °C for longer time were delaminated. The growth in oxide developed stresses that influence the mechanical as well as protective properties of the scale. During growth, re-crystallization may occur in either metal or oxide to alter the stress situation radically. Thus the growth of chromium oxide at the interface of bond coat and top coat increased the stress level (Ref 5) and initiated a crack which propagated easily in a structurally weak top coat. The top coat was structurally weak because large number of porosity was present.

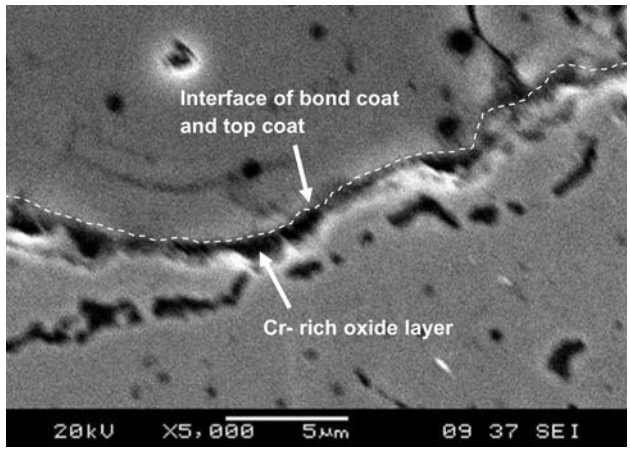


**Fig. 6** Chromium-rich oxide layer in sample treated at 800 °C for 100 h

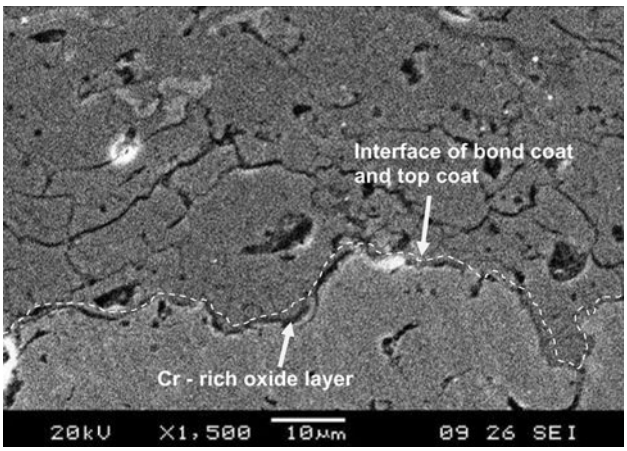


**Fig. 5** Interface of bond coat and top coat after exposure at 700 °C for 100 h

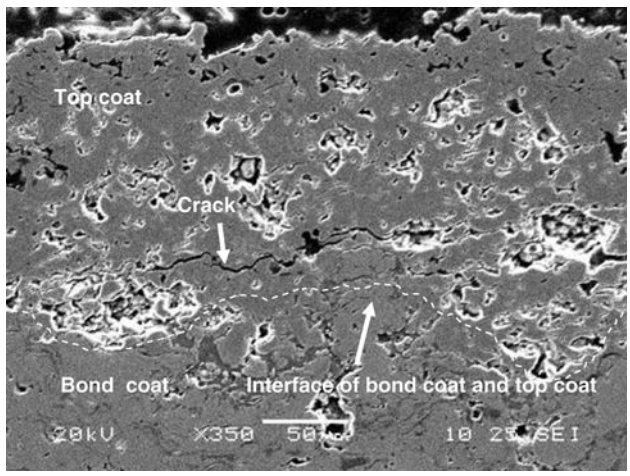


**Fig. 7** Crack formation in sample treated at 800 °C for 100 h

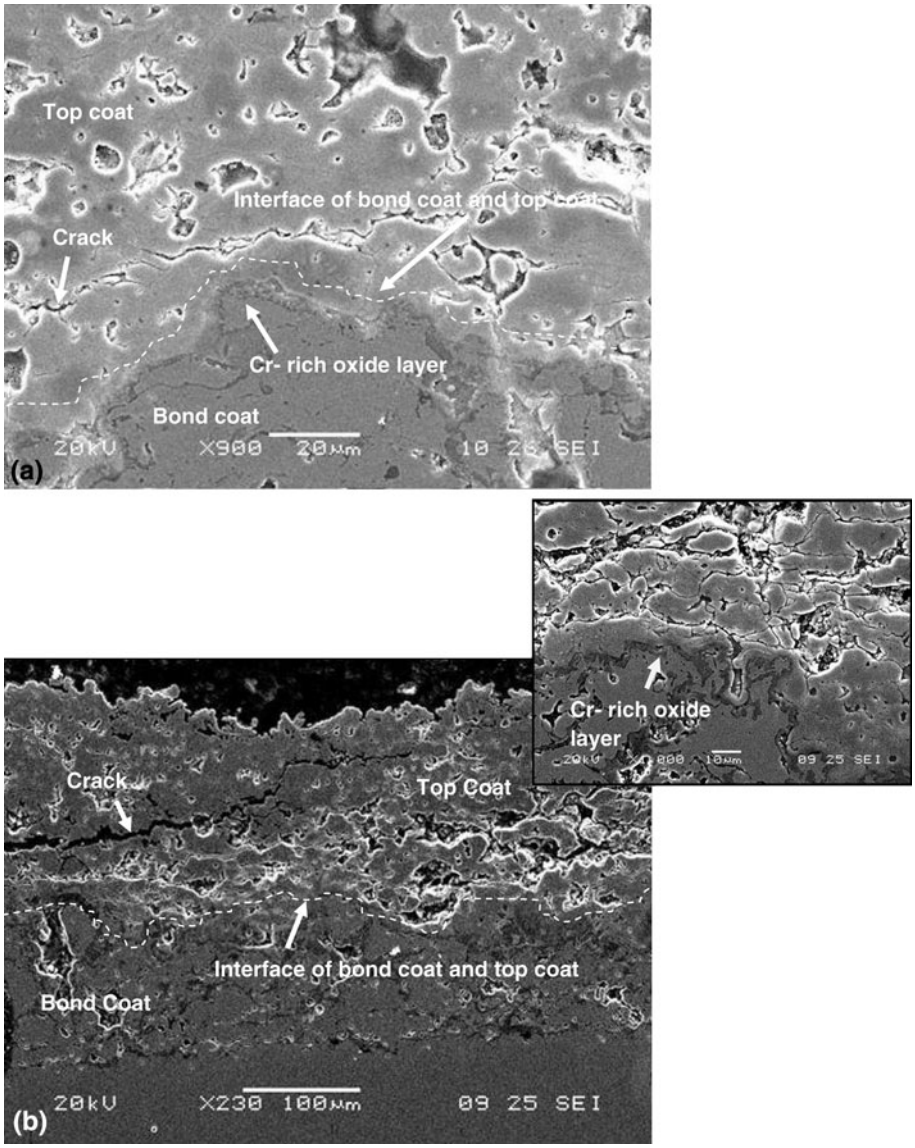


**Fig. 8** (a) Crack growth as function of time for sample treated at 900 °C for 10 h. (b) Crack growth as function of time for sample treated at 900 °C for 20 h

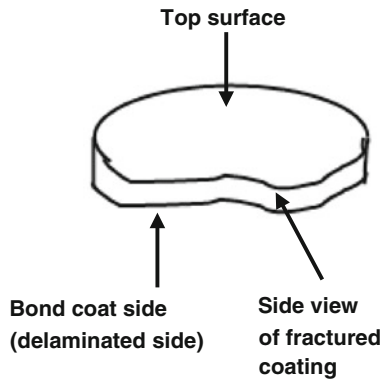


**Fig. 9** Schematic of delaminated top coat

It was further noticed that the samples exposed at 900 °C started to delaminate layer by layer from the top surface, Fig. 13. The probable reason of this phenomenon is explained in section of phase analysis.

There was no apparent affect on the substrate and bond coat interface at 700 and 800 °C, however, at high temperature it revealed that the diffusion of different elements took place. The concentration profiles were estimated for Fe, Ni, and Cr across bond coat and substrate interface as these elements showed high mobility. It was observed that the sample treated at 700 °C showed no diffusion of elements even after 100 h. However, after exposure at 800 °C for 100 h (Fig. 14a) and 900 °C for 20 h (Fig. 14b), it was revealed that the Fe diffused into bond coat and Ni diffused out to substrate. This elemental

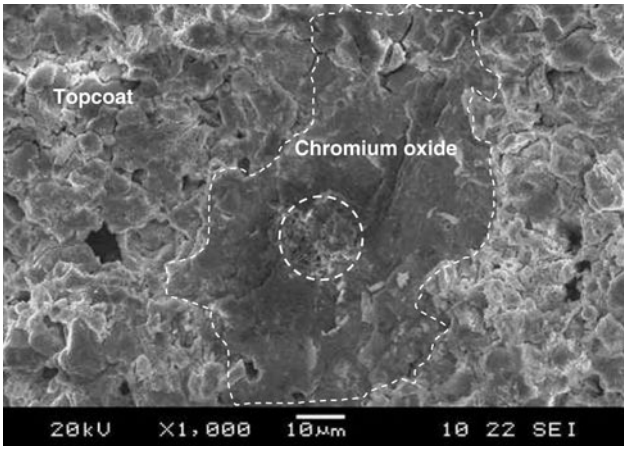


**Fig. 10** Delaminated top coat showing the interface of top coat and bond coat. The chromium oxide region present at the centre of the coating, some portion of bond coat (encircled) still intact

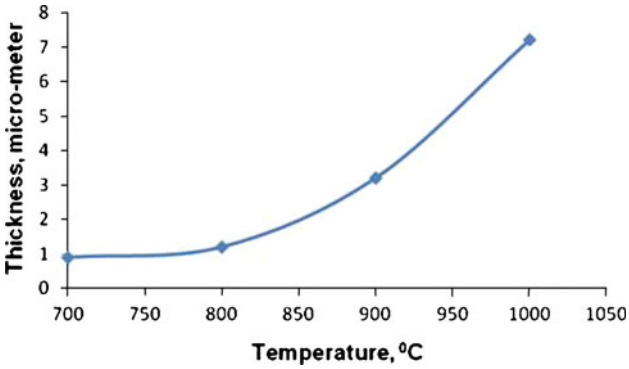


**Fig. 11** Change in thickness of chromium-rich oxide layer with temperature

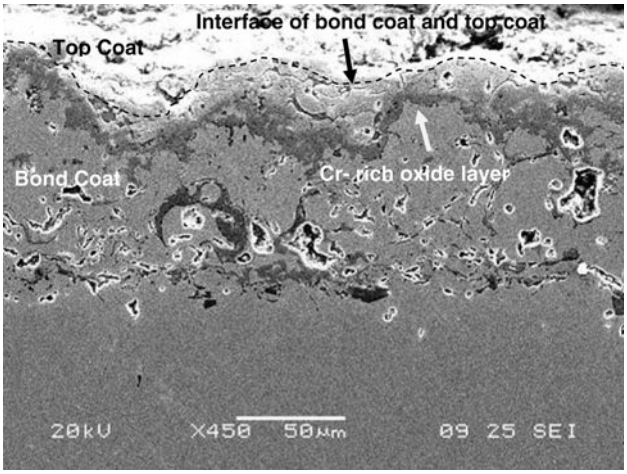


**Fig. 12** Chromium-rich oxide layer in sample heat treated at 1000 °C for 20 h

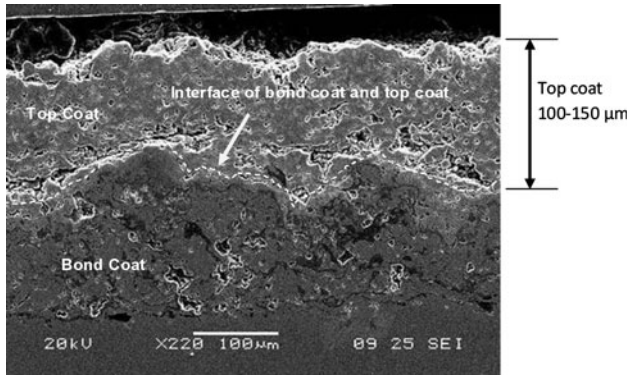


**Fig. 13** Cross-sectional side of samples heat treated at 900 °C for 20 h

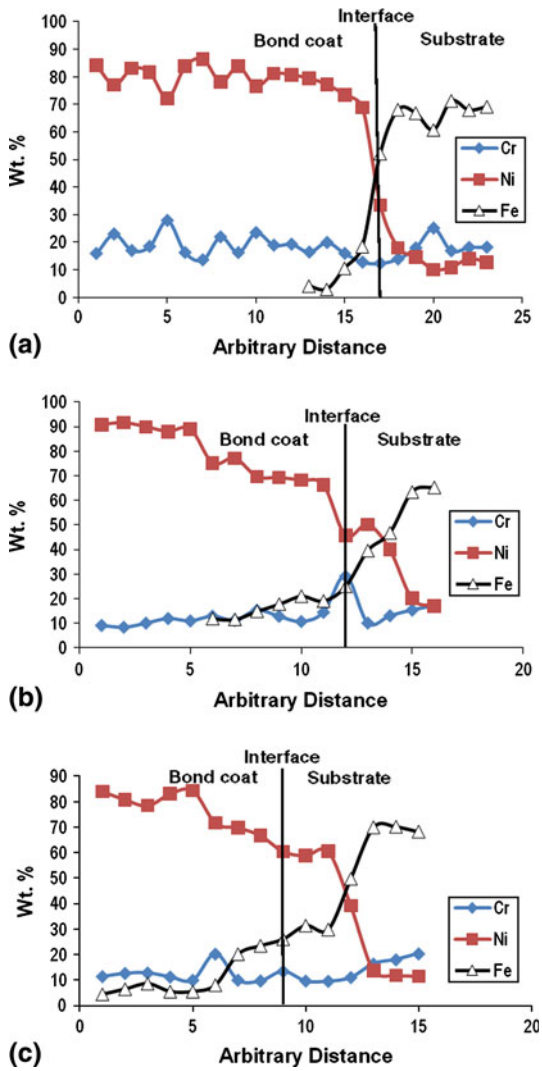


**Fig. 14** (a) Chemical composition profiles across the bond coat and substrate interface for samples heat treated at 800 °C for 100 h. (b) Chemical composition profiles across the bond coat and substrate interface for samples heat treated at 900 °C for 20 h. (c) Chemical composition profiles across the bond coat and substrate interface for samples heat treated at 1000 °C for 20 h

diffusion of Fe and Ni at the interface of bond coat and substrate clearly affects the mechanical/adhesion properties of the coating. At 1000 °C, the mobility of elements became more significant, Fig. 14c, and after 20 h Fe and Ni are clearly diffused from substrate to bond coat and bond coat to substrate, respectively.

### 3.2 Fractrography

Microstructure observations were also made on the fracture surface of the top coat. For this purpose the top coat was fractured and fresh fracture surface was observed under the SEM.

It was revealed in as-sprayed top coat, that the thickness of lamellas was not more than 3 μm, taking the shape of substrate contours. A columnar microstructure was observed within the lamella, growing from bottom to top, indicating the heat deception direction. It was noted that the thickness of the individual columnar grain was about 40 ± 20 nm, Fig. 15.

It was also observed that a lot of smooth features (Fig. 16) were present within the coating indicating that these were porosities which revealed upon fracture. Some cracks were also found within the fracture which might be formed during stress relaxation on solidification of semi-molten splats.

Samples treated at high temperature demonstrated an interesting feature; it was observed that a fine elongated microstructure present within the splat grew in thickness after long exposure at high temperature, Fig. 17. The thickness of the elongated grain for as-sprayed coating was only 40 ± 20 nm which became 90 ± 30 nm after 60 h at 900 °C. The growth of structure is an important aspect because it may affect the mechanical properties of the top coat.

Further, it was noted that the cracks present in the as-sprayed coated sample became more prominent upon thermal treatment, Fig. 18. This may be due to relaxation of stresses which were still present in the coating. The coatings treated at high temperatures, i.e., 900 and 1000 °C also showed sintering features, Fig. 19.

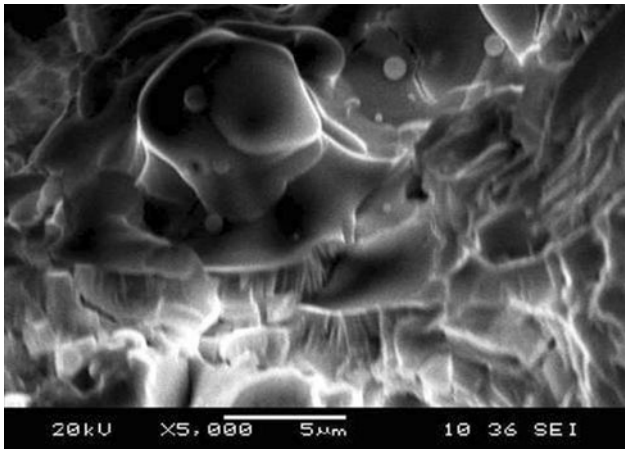


**Fig. 16** The fractured surface of the top coat of as-sprayed sample showing the smooth features and cracks

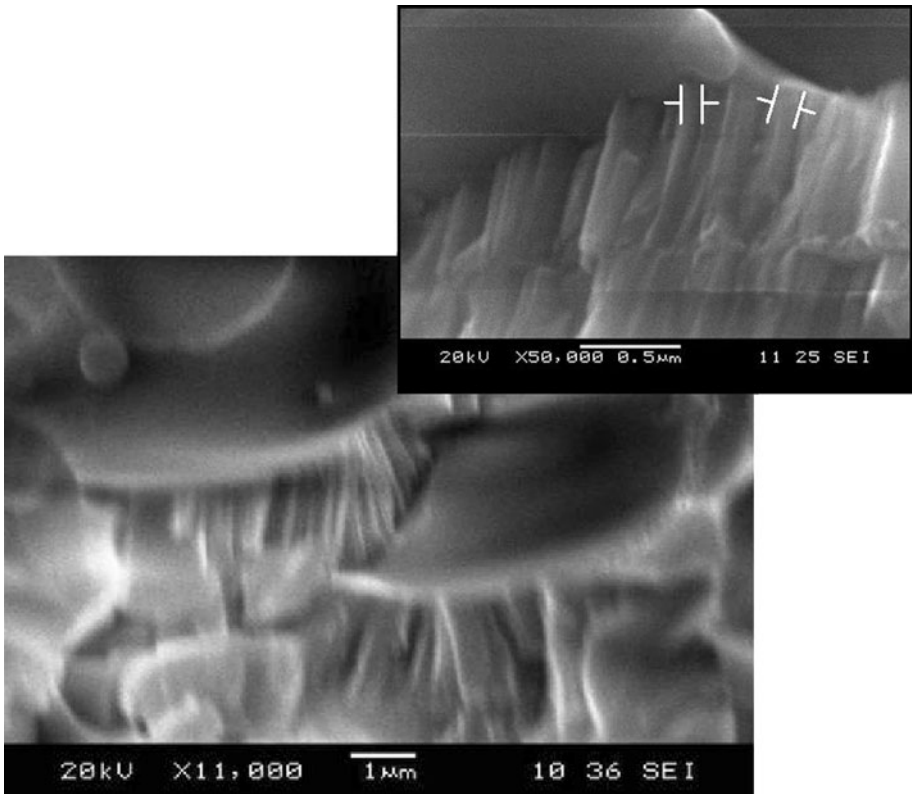


**Fig. 15** The fractured surface of the top coat of as-sprayed sample

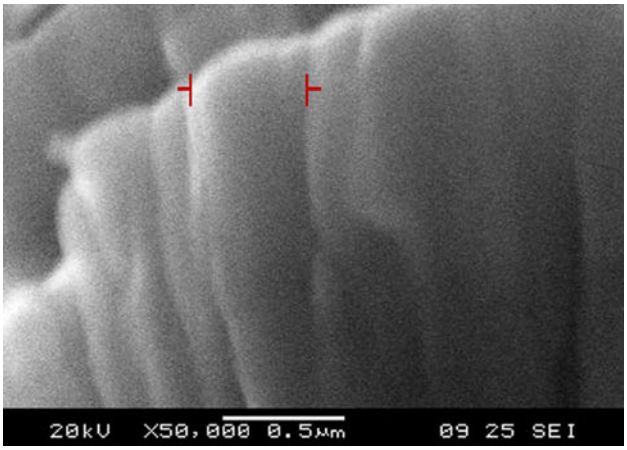


**Fig. 17** The columnar structures after 60 h exposure at 900 °C

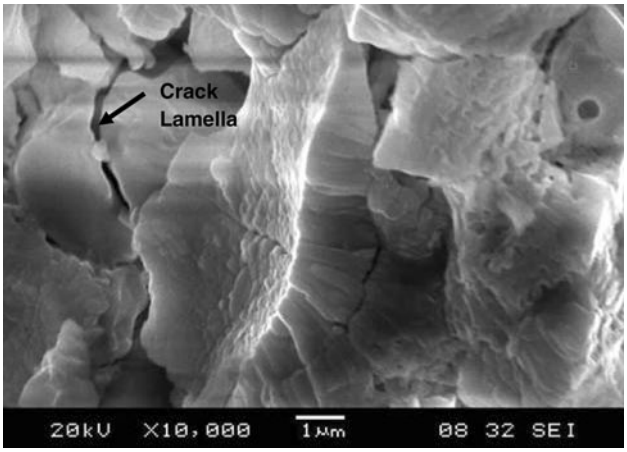


**Fig. 18** The cracked lamella observed after 100 h exposure at 900 °C

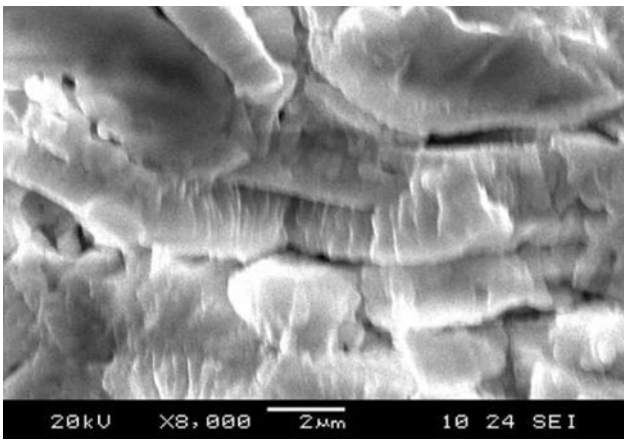


**Fig. 19** Sintering features observed after 40 h exposure at 1000 °C

### 3.3 Phase Analysis

In as-sprayed samples, the XRD results revealed that the top coat is made up of ortho-rhombic phase with minor amount of cubic phase (Fig. 20). Formation of cubic phase in top coat was not due to melting and spraying but was already present in the calcium zirconate powder, Fig. 20.

The top coat when isothermally heat treated at 700 °C showed no change in metallurgical phases and remained same after 100 h, Fig. 21. At 800 °C, in the first few hours, no change in phase was observed but after 10 h exposure small amount of metastable monoclinic $CaZr_4O_9$ phase

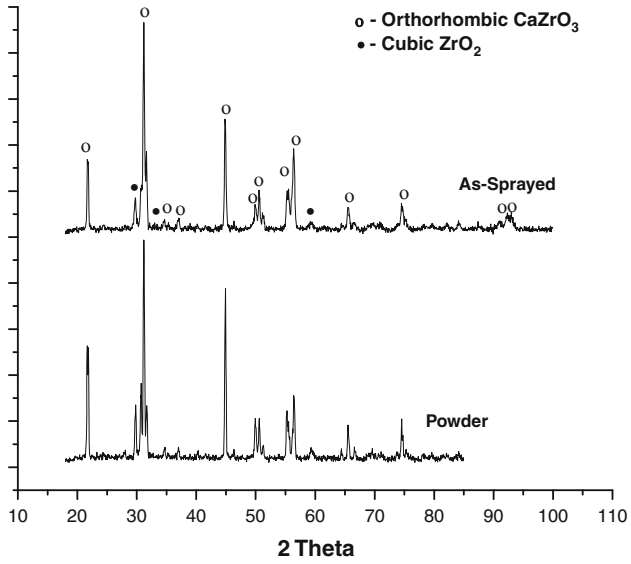


**Fig. 20** XRD pattern of as-sprayed sample with powder sample showing $CaZrO_3$ and cubic phase

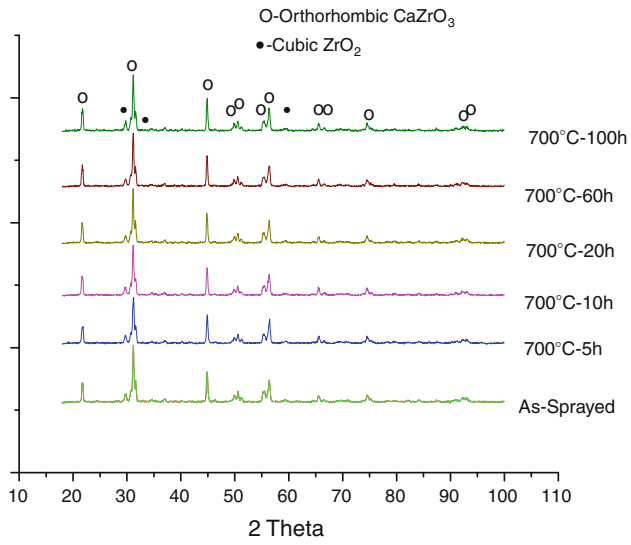


**Fig. 21** Comparison of XRD patterns for the samples exposed at 700 °C for different times with as-sprayed sample

appeared, Fig. 22. The amount of $CaZr_4O_9$ continuously increased and after 100 h of exposure it became 47%. The phase transformation is further evident in sample heat treated at 900 °C for 20 h, Fig. 23, and $CaZr_4O_9$ was measured up to 64%.

The diffraction of main peaks for the $d$ values, $d = 3.14$ and $d = 1.94$ for monoclinic phase and $d = 2.86$ for orthorhombic phase were found in the 2θ range between 28.4° and 46.9°. The volume fraction, $V_m$ of the monoclinic phase was calculated according to the Toraya et al. (Ref 32, 33) method, where $V_m$ is:

$$V_m = P \cdot X_m / 1 + (P - 1)X_m \quad \text{(Eq 1)}$$

where the value of $P$ was calculated by Toraya et al. (Ref 32, 33), as 1.3 and for the monoclinic-tetragonal system, $X_m$ is the integrated intensity ratio defined by:

$$X_m = I_m(d = 3.14) + I_m(d = 1.94)/I_m(d = 3.14) + I_m(d = 1.94) + I_o(d = 2.86) \quad \text{(Eq 2)}$$

where $I$ is the integrated intensity from the monoclinic (m) and orthorhombic (o) phases.

It seems that there is a great role of $CaZr_4O_9$ phase in delamination of the top layers of top coat. $CaZr_4O_9$ is a meta-stable monoclinic phase (Ref 26), generally the formation of monoclinic phase is associated with volumetric changes. The transformation of orthorhombic to monoclinic are associated with stresses which leads to delamination of the upper most layers of the top coat. The formation of $CaZr_4O_9$ started to form preferentially in those regions which were maximum exposed to atmosphere at high temperature. However, it is interesting to note that the complete delamination of the top coat is not due to the formation of meta-stable monoclinic phase since no such phase was observed on the delaminated side of the topcoat, Fig. 24.

The samples exposed at 1000 °C showed no formation of $CaZr_4O_9$ phase after long exposure, Fig. 25, This is, as explained earlier, due to the fact that meta-stable monoclinic formed on the surface quickly and then forced the upper most layers of the top coat to delaminate and newly exposed surface, which left over, not demonstrated peak of $CaZr_4O_9$.

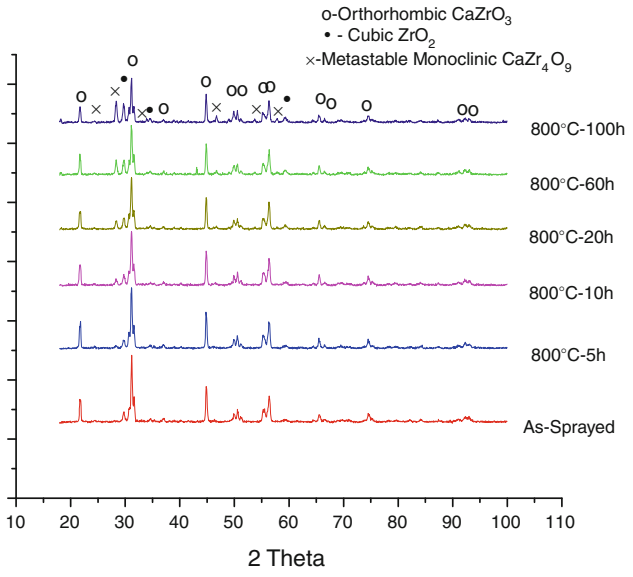


**Fig. 22** Comparison of XRD patterns for the samples exposed at 800 °C for different times and the as-sprayed sample. The emergence of $CaZr_4O_9$ is visible at different stages

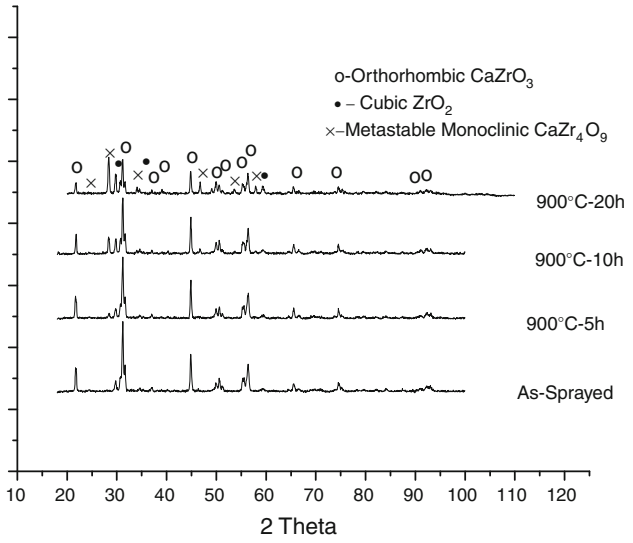


**Fig. 23** Comparison of XRD pattern showing the emergence of $CaZr_4O_9$ phase at 900 °C for different exposure time

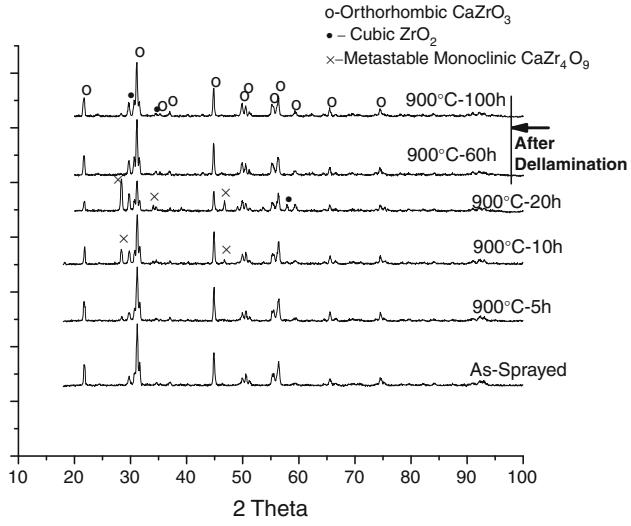


**Fig. 24** Comparison of XRD pattern showing the emergence of $CaZr_4O_9$ phase at 900 °C for 5, 10, and 20 h and absence of $CaZr_4O_9$ phase after delamination when exposed at 900 °C for 60 and 100 h

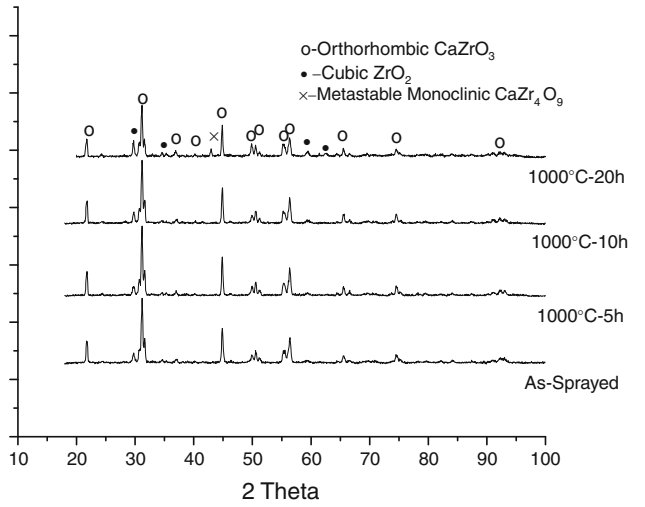


**Fig. 25** XRD pattern for the sample heat treated at 1000 °C for 5, 10, and 20 h comparing with as-sprayed sample

## 4. Conclusions

- The 31% CaO-stabilized zirconia coating demonstrated that there is no significant affect up to 700 °C for 100 h of exposure. However, increase in temperature drastically deteriorates the top coat.
- The columnar grains observed in lamella were continually grown with time and temperature.
- Two modes of top coat failures were observed in CaO-stabilized zirconia coating. Firstly, layer by layer delamination of top coat and secondly, the complete delamination of the top coat at the interface of the bond coat and top coat. The first type of failure was due to the formation of metastable monoclinic, $CaZr_4O_9$ phase and the second was due to the growth of chromium-rich oxide layer.
- The bond coat and substrate interface demonstrated the diffusion of different elements which may alter the mechanical properties of interface.

### References


1. S. Bose, *High Temperature Coatings*, Elsevier Science & Technology Books, Butterworth-Heinemann, ISBN: 0750682523, 2007
2. N.P. Padture, M. Gell, and E.H. Jordan, Thermal Barrier Coatings for Gas-Turbine Engine Applications, *Science*, 2002, **296**(5566), p 280-284
3. A. Rico, J.G. Garcia, C.J. Munez, P. Poza, and V. Utrilla, Mechanical Properties of Thermal Barrier Coatings After Isothermal Oxidation. Depth Sensing Indentation Analysis, *Surf. Coat. Technol.*, 2009, **203**, p 2307-2314
4. G. Guidoni, A. Dudek, S. Patsias, and M. Anglada, Fracture Behaviour of Thermal Barrier Coatings After High Temperature Exposure in Air, *Mater. Sci. Eng.*, 2005, **A397**, p 209-214
5. M.J. Pomeroy, Coatings for Gas Turbine Materials and Long Term Stability Issues, *Mater. Des.*, 2005, **26**, p 223-231
6. Y.Q. Wang and G. Sayre, Commercial Thermal Barrier Coatings with a Double-Layer Bond Coat on Turbine Vanes and the Process Repeatability, *Surf. Coat. Technol.*, 2009, **203**, p 2186-2192
7. E. Garcia, C. Cano, T.W. Coyle, M.I. Osendi, and P. Miranzo, Thermally Sprayed $CaZrO_3$ Coatings, *J. Therm. Spray Technol.*, 2008, **17**(5–6), p 865-871
8. E. Withey, C. Petorak, R. Trice, G. Dickinson, and T. Taylor, Design of 7 wt.% $Y_2O_3$-$ZrO_2$/Mullite Plasma-Sprayed Composite Coatings for Increased Creep Resistance, *J. Eur. Ceram. Soc.*, 2007, **27**, p 4675-4683
9. H. Zhou, F. Li, B. He, J. Wang, and B.D. Sun, Air Plasma Sprayed Thermal Barrier Coatings on Titanium Alloy Substrates, *Surf. Coat. Technol.*, 2007, **201**, p 7360-7367
10. Y. Bai, Z.H. Han, H.Q. Li, C. Xu, Y.I. Xu, C.H. Ding, and J.F. Yang, Structure-Property Differences Between Supersonic and Conventional Atmospheric Plasma Sprayed Zirconia Thermal Barrier Coatings, *Surf. Coat. Technol.*, 2011, **205**(13-14), p 3833-3839
11. M. Saremi, A. Afrasiabi, and A. Kobayashi, Microstructural Analysis of YSZ and YSZ/$Al_2O_3$ Plasma Sprayed Thermal Barrier Coatings After High Temperature Oxidation, *Surf. Coat. Technol.*, 2008, **202**, p 3233-3238
12. A. Portinha, V. Teixeira, J. Carneiro, J. Martins, M.F. Costa, R. Vassen, and D. Stoever, Characterization of Thermal Barrier Coatings with a Gradient in Porosity, *Surf. Coat. Technol.*, 2005, **195**, p 245-251
13. T. Lauwagie, K. Lambrinou, S. Patsias, W. Heylen, and J. Vleugels, Resonant-Based Identification of the Elastic Properties of Layered Materials: Application to Air-Plasma Sprayed Thermal Barrier Coatings, *NDT&E Int.*, 2008, **41**, p 88-97
14. R. Vaben, M.O. Jarligo, T. Steinke, D.E. Mack, and D. Stover, Overview on Advanced Thermal Barrier Coatings, *Surf. Coat. Technol.*, 2010, **205**, p 938-942
15. P. Mohan, T. Patterson, V.H. Desai, and Y.H. Sohn, Degradation of Free-Standing Air Plasma Sprayed CoNiCrAlY Coatings by Vanadium and Phosphorus Pentoxides, *Surf. Coat. Technol.*, 2008, **203**, p 427-431
16. H. Liu, S. Li, Q. Li, Y. Li, and W. Zhou, Microstructure, Phase Stability and Thermal Conductivity of Plasma Sprayed $Yb_2O_3$, $Y_2O_3$ Co-Stabilized $ZrO_2$ Coatings, *Solid State Sci.*, 2011, **13**(3), p 513-519
17. T. Patterson, A. Leon, B. Jayaraj, J. Liu, and Y.H. Sohn, Thermal Cyclic Lifetime and Oxidation Behavior of Air Plasma Sprayed CoNiCrAlY Bond Coats for Thermal Barrier Coatings, *Surf. Coat. Technol.*, 2008, **203**, p 437-441
18. K.W. Schlichting, N.P. Padture, E.H. Jordan, and M. Gell, Failure Modes in Plasma-Sprayed Thermal Barrier Coatings, *Mater. Sci. Eng.*, 2003, **A342**, p 120-130
19. A.J. Burns, R. Subramanian, B.W. Kempshall, and Y.H. Sohn, Microstructure of As-Coated Thermal Barrier Coatings with Varying Lifetimes, *Surf. Coat. Technol.*, 2004, **177--178**, p 89-96
20. U. Schulz, C. Leyens, K. Fritscher, M. Peters, B.S. Brings, O. Lavigne, J.M. Dorvaux, M. Poulain, R. Mevrel, and M. Caliez, Some Recent Trends in Research and Technology of Advanced Thermal Barrier Coatings, *Aerosp. Sci. Technol.*, 2003, **7**, p 73-80
21. A.C. Fox and T.W. Clyne, Oxygen Transport by Gas Permeation Through the Zirconia Layer in Plasma Sprayed Thermal Barrier Coatings, *Surf. Coat. Technol.*, 2004, **184**, p 311-321
22. A.N. Khan and J. Lu, Thermal Cyclic Behavior of Air Plasma Sprayed Thermal Barrier Coatings Sprayed on Stainless Steel Substrate, *Surf. Coat. Technol.*, 2007, **201**, p 4653-4658
23. W.Z. Wang, C.J. Li, and Y.Y. Wang, Effect of Spray Distance on the Mechanical Properties of Plasma Sprayed Ni-45Cr Coatings, *Mater. Trans.*, 2006, **47**(7), p 1643-1648
24. W. Beele, G. Marijnissen, and A.V. Lieshout, The Evolution of Thermal Barrier Coatings-Status and Upcoming Solutions for Today's Key Issues, *Surf. Coat. Technol.*, 1999, **120--121**, p 61-67
25. X.Q. Cao, R. Vassen, and D. Stoever, Ceramic Materials for Thermal Barrier Coatings, *J. Eur. Ceram. Soc.*, 2004, **24**, p 1-10
26. C. Cano, M.I. Osendi, M. Belmonte, and P. Miranzo, Effect of the Type of Flame on the Microstructure of $CaZrO_3$ Combustion Flame Sprayed Coatings, *Surf. Coat. Technol.*, 2006, **201**, p 3307-3313

27. I. Taymaz, An Experimental Study of Energy Balance in Low Heat Rejection Diesel Engine, *Energy*, 2006, **31**(2–3), p 364-371
28. E. Buyukkaya, T. Engin, and M. Cerit, Effects of Thermal Barrier Coating on Gas Emissions and Performance of a LHR Engine with Different Injection Timings and Valve Adjustments, *Energy Convers. Manag.*, 2006, **47**, p 1298-1310
29. T. Goto, Thermal Barrier Coatings Deposited by Laser CVD, *Surf. Coat. Technol.*, 2005, **198**(1–3), p 367-371
30. S. Guo, Y. Tanaka, and Y. Kagawa, Effect of Interface Roughness and Coating Thickness on Interfacial Shear Mechanical Properties of EB-PVD Yttria-Partially Stabilized Zirconia Thermal Barrier Coating Systems, *J. Eur. Ceram. Soc.*, 2007, **27**, p 3425-3431
31. W.R. Chen, X. Wu, D. Dudzinski, and P.C. Patnaik, Modification of Oxide Layer in Plasma-Sprayed Thermal Barrier Coatings, *Surf. Coat. Technol.*, 2006, **200**, p 5863-5868
32. A.N. Khan, J. Lua, and H. Liao, Heat treatment of Thermal Barrier Coatings, *Mater. Eng.*, 2003, **A359**, p 129-136
33. H. Toraya, M. Yoshirmura, and S. Somiya, Calibration Curve for Quantitative Analysis of the Monoclinic-Tetragonal $ZrO_2$ System by X-Ray Diffraction, *J. Am. Ceram. Soc.*, 1984, **67**, p C119-C121